Nanoscale

Accepted Manuscript

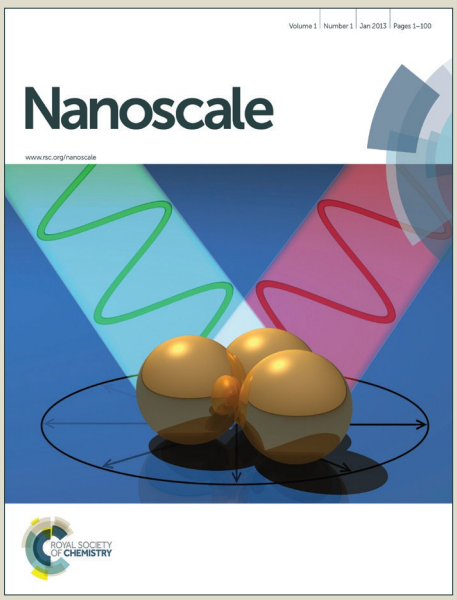

ROYAL SOCIETY OF CHEMISTRY

www.rsc.org/nanoscale

Image charge effect and vibron-assisted processes in Coulomb blockade transport: a first principles approach

A. M. Souza,[1*] I. Rungger,[1†] U. Schwingenschlögl[2] and S. Sanvito[1]
[1]*School of Physics, CRANN and AMBER, Trinity College, Dublin 2, Ireland and*
[2]*PSE Division, KAUST, Thuwal 23955-6900, Saudi Arabia*

We present a combination of density functional theory and of both non-equilibrium Green's functions formalism and a Master equation approach to accurately describe quantum transport in molecular junctions in the Coulomb blockade regime. We apply this effective first-principles approach to reproduce the experimental results of Perrin *et al.,* [Nature Nanotech. **8**, 282 (2013)] for the transport properties of a Au-(Zn)porphyrin-Au molecular junction. We demonstrate that energy levels renormalization due to the image charge effect is crucial to predict the current onset in the current-voltage, I-V, curves as a function of the electrodes separation. Furthermore, we show that for voltages beyond that setting the current onset the slope of the I-V characteristics is determined by the interaction of the charge carriers with molecular vibrations. This corresponds to current-induced local heating, which may also lead to an effective reduced electronic coupling. Overall our scheme provides a fully *ab initio* description of quantum transport in the Coulomb blockade regime in the presence of electron-vibron coupling.

Mechanically controlled break junctions (MCBJs), where the target molecule bridges two metallic electrodes, have been widely used to measure the transport properties of organic compounds[1–11]. In all these junctions an organic/inorganic interface is formed, and the detailed understanding of its electronic properties is crucial to interpret the experimental data.[12–14] Depending on how the molecule connects to the electrodes, two main transport regimes can take place. For strong electronic coupling fractional charge transfer can occur and in this case the occupation of some molecular levels may be on average, non-integer. In contrast, Coulomb blockade (CB) dominates for weak coupling,[15] and the transport is characterized by tunnelling of an integer number of electrons.

In addition, even for weak coupling, it is experimentally known[16–19] that the quasi-particle energy gap of a molecule, $E^{\rm gap}$, is reduced with respect to its gas phase value upon the formation of the interface. Here $E^{\rm gap}$ is defined as the difference between the molecule ionization potential, $I_{\rm P}$, and its electron affinity, $E_{\rm A}$.The effect is mainly due to the Coulomb interaction between the added (subtracted) charge on the molecule and the screening holes (electrons) on the substrate. Such interaction leads to a polarization of the surface, so that a charge with opposite sign with respect to that of the molecule is formed. This non-local form of charge correlation is called image-charge effect, and it becomes more relevant for small molecule-substrate distances,[12,20] leading to a strong renormalization of the energy levels and consequently to a reduction of $E^{\rm gap}$ upon the molecule approaching the surface. Although this effect is expected to be present in all transport measurements through molecules, only recently it was experimentally verified in a direct way. Using MCBJs Perrin *et al.*[1] were able to observe the energy levels renormalization of a zinc porphyrin molecule [Zn(5,15-di(p-thiolphenyl)-10,20-di(p-tolyl)porphyrin) in short ZnTPPdT] weakly coupled to two gold electrodes. The experiments observed a shift of the current onset upon stretching the junctions, i.e. upon changing the distance between the molecule and the electrodes surface.

From a theoretical point of view the transport properties of molecular junctions are mostly studied with the non-equilibrium Green's functions (NEGF) formalism,[21–23] often implemented with Kohn-Sham (KS)[24] density functional theory (DFT)[25]. This approach, however, presents some limitations. Firstly, the KS eigenvalues cannot be rigorously interpreted as the quasi-particle energies of a system, and even if such interpretation is imposed, they usually do not represent in a quantitatively accurate way the excitation spectrum of molecules. Concerning the image charge effect, the standard approximations to the exchange and correlation (XC) functional, such as the local density approximation (LDA)[26], the generalized gradient approximation (GGA),[27] hybrid functionals[28] or explicitly self-interaction corrected functionals,[29,30] do not include non-local correlation effects. As such, in general, they are not capable to capture the renormalization of the molecular energy levels when a molecule approaches a metallic surface.[12,20,31] Many-body methods based on the GW approximation have been successfully applied to this problem, however, due to its computational overheads, it becomes impractical for system larger than a few hundred atoms.[32–34] Finally, the lack of the derivative discontinuity[35–37] in the DFT-LDA potential makes the energy levels position linearly dependent on their occupation, so that the molecular levels can be fractionally occupied even in the weak coupling limit. This means that the Coulomb blockade regime cannot be described by

*Present address: Johannes Gutenberg University, Institute of Physics, Spice Centre, Germany.
†Present address: National Physical Laboratory, Hampton Road, TW11 OLW, United Kingdom.

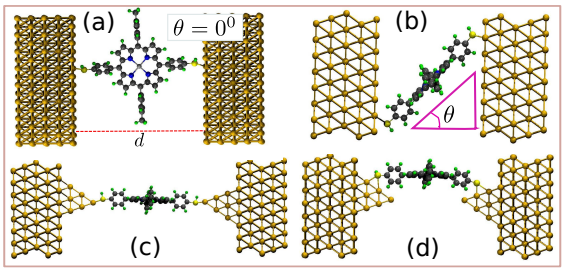

Figure 1: Ball-and-stick representation of a Au-ZnTPPdT(thiol)-Au molecular junction. Panels (a) and (b) show the equilibrium and a compressed geometry for the molecule sandwiched between two flat surfaces. In (b) the molecule tilts and makes an angle θ with the transport direction. Panels (c) and (d) show two junctions when two tip electrodes are considered. The molecule is attached on top of the two gold tips.

NEGF-DFT. Different approaches have been developed to circumvent this limitation, e.g, by including electron-electron interaction within a model Hamiltonian[38,39] to be used within the NEGF and corrections for the self-interaction error.[40]

Here we present a computationally efficient approach combining first-principles calculations and a master equation (ME) formulation,[15,41–44] which is capable of describing the effects of strong correlation and molecule vibrations on the junction conduction. The electronic parameters for the ME are all extracted from NEGF-DFT in the LDA, with appropriate corrections for energy level renormalisation. Instead we simplify the treatment of the vibrons by considering a single vibrational mode and by taking the electron-vibron coupling as a free parameter. Such an approach is used to investigate the current-voltage, I-V, characteristics of a ZnTPPdT molecule sandwiched between two Au surfaces (the Au-ZnTPPdT-Au junction) as a function of the separation between the electrodes. The energy level renormalisation of the molecule approaching the surface is calculated by a classical electrostatic model, where the image plane height needed in the model is obtained from constrained DFT (cDFT) calculations. In this way the renormalization of the energy levels is captured fully from first principles, without resorting to parameters. Then the levels broadening is evaluated with NEGF-DFT at the corrected energy levels. Such information is input into the ME, which is then capable of correctly describing the bias corresponding to the current onset for the various junctions. Finally, the inclusion of vibrons allows us to reproduce I-V profile for bias voltages beyond that corresponding to the current onset. Our results are directly compared with the experimental data,[1] demonstrating an extremely good agreement.

We start by discussing our NEGF-DFT results obtained at the level of the LDA. The Au electrodes are modeled by considering a five layer thick 8×8 supercell terminated with a (111) surface. The geometry of the molecule in the gas phase is first relaxed by conjugate gradient, and then the structure obtained is placed into the junction and connected to two flat electrodes at a hollow site. In our calculations we use periodic boundary conditions in all directions, however along the vertical direction [see Fig. 1(a)] we add a vacuum region of about 10 Å between the Au electrodes in order to separate the periodic images of the molecules and avoid spurious interactions. Also the lateral dimensions of our supercell have been chosen so to avoid interaction between the molecule and its periodic replica. The equilibrium distance between the two Au surfaces[1] is $d_{\mathrm{Au-Au}} = 23.2$ Å[see Fig. 1(a)]. Since both thiol and thiolate terminations of the molecule are possible[12], here we have considered both cases. Furthermore, we have investigated alternative electrodes morphologies, by looking at tip-terminated Au surfaces as shown in Fig. 1(c) and Fig. 1(d). This allows us to understand the effects of the contact geometry on the electronic coupling between the molecule and the electrodes. In order to study the effect of the image charge as a function of $d_{\mathrm{Au-Au}}$, three new configurations are built, where the molecule is rigidly tilted forming an angle, θ, relative to the straight equilibrium configuration, as shown in Fig. 1(b). Notably, in MCBJs experiments the molecule accesses many different meta-stable configurations due to the rearrangement of the atoms during the stretching of the junction and we have addressed this in the past[13,14] by means of molecular dynamics simulations. Although these geometrical rearrangements can lead to quantitatively differences in the transport properties the qualitative features remains unchanged. Here however we consider only the discussed idealized structures, with the aim of resolving the main transport mechanisms taking place in such junctions from first principles.

Fig. 2(a) and Fig. 2(b) show the transmission coefficients, $T(E)$, computed with NEGF-DFT at the LDA level as a function of energy for the thiol and thiolate terminations, respectively, and for different values of θ. For $\theta = 0$ (equilibrium distance) the resonance corresponding to the KS highest-occupied molecular orbital (HOMO) is at 0.49 eV below the Fermi level, E_{F}, for the thiol-terminated junction, and at 0.2 eV for the thiolate ones. Since in both cases the HOMO is the molecular orbital closer to E_{F}, it is the one responsible for the transport at low bias. The broadening of the KS-HOMO for the thiolate-terminated junction is larger than that of the thiol one, indicating a stronger electronic coupling between the molecule and the electrodes. The strength of such electronic coupling is quantified in Table I, where we list Γ_{L} (Γ_{R}), for electron hopping from the left- (right-) hand side electrode to the molecule. These have been extracted from the spectral representation of the Green's function associated to the scattering region in the NEGF-DFT framework.[45]. The most notable feature for both terminations is that the energy positions of the HOMO resonance are insensitive to the value of θ, i.e. they do

not vary with $d_{\mathrm{Au-Au}}$. This confirms the fact that DFT-LDA is not able to capture the renormalization of the energy levels due to the image charge effect. Note that our electrodes are effectively Au slabs, which inherently have a "rough" density of states due to vertical confinement. This "rough" electrodes density of states is then reflected also in the transmission coefficient. Nonetheless, the roughness induced by such a confinement is small compared to the actual transmission peaks dominating the current.

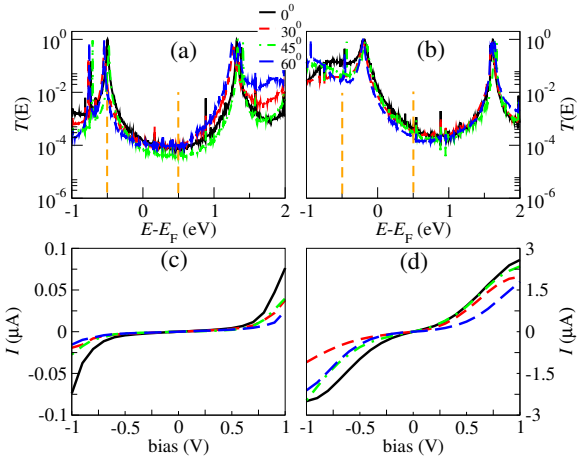

Figure 2: Transport properties of Au-ZnTPPdT(thiol)-Au junctions. The transmission coefficients as a function of energy, $T(E)$, are shown in panel (a) and (b), respectively for the thiol- and thiolate-terminated molecule. The corresponding I-V curve are in panel (c) and (d). The vertical dashed-lines in (a) and (b) mark the bias window for $V = 1$ Volt.

Table I: Electronic couplings between the HOMO and LUMO to the left-hand and right-hand side electrode, obtained from NEGF-DFT at the LDA level. Results are presented for the different values of θ and for both the thiol- and thiolate-terminated junctions. The values of $\Gamma_{\mathrm{L/R}}$ are in meV.

		Thiol				Thiolate			
		HOMO		LUMO		HOMO		LUMO	
Angle (^{0})	$d_{\mathrm{Au-Au}}$(Å)	Γ_L	Γ_R	Γ_L	Γ_R	Γ_L	Γ_R	Γ_L	Γ_R
0	23.2	6.0	5.5	6.5	6.5	19.0	16.0	8.0	8.0
30	19.9	5.7	5.0	8.0	5.0	25.0	8.0	9.0	8.0
45	16.40	6.5	3.5	6.0	3.5	15.0	10.0	7.0	6.0
60	12.9	5.0	3.6	7.0	5.0	12.0	10.0	7.0	7.0

The I-V curves for the thiol- and thiolate-terminated junctions are presented in Fig. 2(c) and Fig. 2(d), respectively. For thiolate termination the current is one order of magnitude larger than that of the thiol-terminated molecule in the same range of applied bias. This is due to the larger $\Gamma_{\mathrm{L/R}}$, as shown in Table I, and to the fact that the HOMO enters the bias window at lower voltages for the thiolate-terminated case [the bias window is marked by the vertical dashed-lines in Fig. 2(a-b)] . We point out here that, since the LDA lacks of the derivative discontinuity of the potential,[29,35,46] the I-V's for both types of junctions do not present a step-like increase of the current at any voltage, but rather appear having a smooth slope. This is because, as the HOMO enters the bias window, its corresponding energy level starts drifting to lower energies. In this way the level remains fractionally occupied and the junction artificially metallic.[40] Since the thiolate-terminated junctions present a systematically larger current than the thiol-terminated ones, and since the currents are typically two orders of magnitude larger than experiments, we conclude that thiol-terminated molecules are likely to be the ones measured in the MCBJ experiments.[1] As such we will focus only on these in the remaining of the paper.

As observed above, the LDA results indicate two main shortfalls of the computational scheme used so far, namely, (i) the renormalization of the energy levels is not captured, and (ii) the lack of the derivative discontinuity of the approximated DFT potential promotes metallic transport. In order to correct for these we apply the ME approach (see computational methods), which allows us to access the weak coupling limit. The ME requires a number of parameters, that here are all calculated by DFT. Let us begin with the quasi-particle energy position, which has to be evaluated by taking into account image charge renormalisation effects. To this goal we consider cDFT combined with a classical model, and evaluate the position of the HOMO as function of $d_{\mathrm{Au-Au}}$.[12,20] Starting from ZnTPPdT(thiol) in the gas phase, we notice that the LDA KS quasi-particle gap, $E^{\mathrm{gap}}_{\mathrm{LDA}}$, is significantly smaller than $E^{\mathrm{gap}}_{\mathrm{QP}} = E_{\mathrm{A}} - I_{\mathrm{P}}$ calculated using the delta self-consistent field (ΔSCF) method.[47] In particular the KS-HOMO is $\sim$1.4 eV higher in energy then $-I_{\mathrm{P}} = -6.39$ eV, while the KS-LUMO is $\sim$1.45 eV lower then $-E_{\mathrm{A}} = -1.74$ eV. The isosurfaces for the HOMO and LUMO are shown in the Fig. S5 in the SI. Similar differences are also found for the ZnTPPdT(thiolate) molecule.

When the molecule is brought close to the metal surfaces the energy levels are renormalised due to the image charge formation. Fig. 3 shows the energies of the frontier molecular orbitals as a function of $d_{\mathrm{Au-Au}}$ (or θ) for ZnPPTdT(thiol) obtained by adding the interaction energy due to the image charge, $U(d)$, to the gas phase $-E_{\mathrm{A}}$ and $-I_{\mathrm{P}}$. This is the potential energy of a point charge interacting with two infinite flat surfaces,[12] which in atomic units reads

$$U(d) = -\frac{Q^2}{2(d/2 - z_0)}\ln 2\,, \qquad (1)$$

where Q is a point charge located at the center of the molecule, $d = d_{\mathrm{Au-Au}}$ is the electrodes separation and z_0 is the height of the image charge plane with respect to the surface atomic positions. We approximate the charge distribution by a point charge placed approximately in the center of the molecule, which has been shown to be a good

approximation.[48] In our case, $z_0 = 1$ Å as obtained by cDFT[12,20] therefore from first-principles, in contrast to other works where z_0 is treated as a free parameter.[48–50] We have demonstrated[20] that this parameter-free model accurately reproduces the energy positions of the frontier molecular orbitals as a function of $d_{\mathrm{Au-Au}}$ calculated by cDFT. Within cDFT these are total energy differences between the ground state and electronic configurations where an integer charge is transferred between the molecule and the metal surface. The data are presented by offsetting the levels by the metal workfunction, $W_{\mathrm{F}} = 5.5$ eV, computed by taking the difference between the vacuum potential and the Fermi energy of a gold slab. The green-dashed lines correspond to the gas phase limit of ZnPPTdT(thiol), i.e. to an infinite separation between molecule and substrate. Note that Δ-SCF can be considered as a special case of the more general cDFT method, in which the molecule is infinitely distant from the surface.

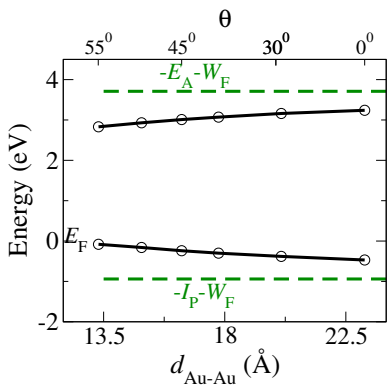

Figure 3: Corrected position of the frontier energy levels of the thiol-terminated junctions with respect to the substrate Fermi energy, E_{F}, which sets the 0 of the energy scale in the figure, as a function of the electrodes separation. We note that for Au we have $E_{\mathrm{F}} = 5.5$ eV, which is equal to the negative of the electrodes workfunction, $W_{\mathrm{F}} = -E_{\mathrm{F}}$. The dashed-green lines indicate $-E_{\mathrm{A}}$ and $-I_{\mathrm{P}}$ offset by E_{F} showing the molecule gas phase limit, i.e. the case of infinite molecule-electrode separation.

Beside the quasi-particle energies the ME approach requires knowledge of the electronic coupling of the molecular levels with the electrodes, Γ_α (α =L,R). As explained before these can be extracted from the spectral representation of the Green's function in the NEGF-DFT formalism. However, the coupling depends not just on the geometrical details of the molecule-surface contact, but also on the exact energy position of a given level.[45] As such it cannot be simply extracted from the LDA Green's function, since the KS levels of the frontier molecular orbitals are usually misplaced. Instead one has first to correct the energy levels position and then to calculate the Γ's. Our approach then consists in two steps. Firstly, we shift the molecular energy levels to the positions calculated with cDFT [those plotted in Fig. 3] by applying to the KS-LDA spectrum a scissor operator (SCO)[12,48] [see supplementary information (SI) for details]. Then the Γ_α's of the corrected states are extracted by fitting the new transmission function, $T(E)$, to a Lorentzian[51] according to Eq. (13) in the SI. Note that in our case the energy position for the frontier energy levels are obtained from cDFT-calculated total energy differences and therefore they contain implicitly also the interaction energies, U, between the added electron and the other electrons on the molecule and the electrodes. The Γ_α's can also depend on the applied bias due to small variations in the density of states of the metal surface as a function of energy. However, we find that the electronic coupling changes by at most 20% when ramping up the bias from 0 V to 2 V. Therefore, we can consider the electronic couplings constant with bias and assume the wide-band approximation [see Eq. (14) in the SI]. Note that in the weak coupling limit fitting the transmission coefficient to a Lorentzian is equivalent to extracting the Γ's from the Green's function.

The left panel of Fig. 4 shows an example of such procedure for the case of the thiol-terminated junction at the equilibrium position ($\theta = 0$). In the case of the LDA (black solid line) the KS-HOMO is 0.5 eV below the electrodes' E_{F}, whereas the molecule $-I_{\mathrm{P}}$ for the gas phase is at 1 eV below E_{F}. However, the image charge correction is 0.53 eV [see Eq. (1)], which brings $-I_{\mathrm{P}}$ for the molecule in the junction to 0.47 eV. Therefore, due to a fortuitous error cancellation, the HOMO as calculated by the LDA coincides with the corrected energy position of $-I_{\mathrm{P}}$. In contrast the position of the KS-LUMO is severely underestimated by the LDA and needs to be shifted to higher energy, namely to 3 eV above E_{F}. The resulting transmission coefficient after such shift is plotted as a blue dashed line in Fig. 4. The same procedure is then followed for different $d_{\mathrm{Au-Au}}$ (different θ) and the resulting Γ_α's for the HOMO and LUMO are shown in Table I. Note that the values obtained from this fitting procedure returns an excellent agreement for the low bias and the saturation current between that calculated with NEGF and that with the master equation (see inset of Fig 4). This confirms that the fitting procedure is accurate to extract the electronic coupling parameters for this system.

The right panel of Fig. 4 shows the I-V curve calculated with NEGF-DFT at the LDA level (black solid line) compared to the total current obtained with the ME when using the calculated parameters (blue solid line, see computational methods for details). As soon as the HOMO enters the bias window at around ±0.9 Volt, the current calculated with the ME shows a sharp step-like increase followed by a plateau. In contrast, the standard NEGF-DFT-calculated I-V is smooth with no sign of saturation. Such behavior is mainly an artefact arising from the lack of derivative discontinuity in the LDA potential. In fact, as the HOMO enters the bias window, it starts to loose charge and drifts to lower energies. The net effect is that the HOMO follows the lowest among

the chemical potentials of the two electrodes, effectively maintaining its fractional charge and carrying significant current. Such energy drift of the HOMO also brings down in energy the LUMO level. Since the LDA gap is severely underestimated, eventually also the LUMO will enter the bias window and will start conducting. This situation is demonstrated in the left panel of Fig. 4 by the LDA transmission coefficient at 2 Volt.

When the finite-bias calculation is not performed self-consistently, i.e. the current is calculated by simply integrating the zero-bias transmission coefficient with a linear potential drop applied between the Au electrodes, then the NEGF-DFT-calculated I-V curve (dashed black line) resembles closely that obtained with the ME. This is due to the fortuitous error cancellation discussed above for the position of the LDA HOMO energy, in which case in a picture of resonant transport through a single molecular level the two approaches will give the same I-V.[52] Note that the non-self-consistent current (black-dashed line) slightly reduces when the applied bias is increased, which means that we observe a negative differential resistance. This is due to the reduction in the transmission coefficient with bias (see Fig. S2 in the SI), which itself is due to a slight reduction of the electronic coupling strength as the applied bias is increased non-selfconsistently. For a self-consistent calculation, in contrast, the electronic couplings increase by 20 % when 2 Volts are applied across the electrodes, showing that the exact change of the electronic couplings with bias depends on the details of the calculation.

In the right panel of Fig. 4 we also show for completeness the individual contributions to the ME-calculated current originating from sequential tunnelling and cotunnelling. In general the transport is dominated by cotunnelling contributions for voltages up to the one corresponding to the high-current onset (see inset), and then it becomes completely determined by sequential tunnelling processes.[52]

Fig. 5 summarizes our main results, obtained by using the ME, for a range of different junctions. The values used for the Γ_α's in Fig. 5(a-b) are given in Table I, while the energy levels positions correspond to those shown in Fig. 3. Since the HOMO is responsible for the transport (the LUMO is too high in energy and does not contribute in the bias range explored), its position with respect to $E_{\rm F}$ determines the conductance gap. This can be easily traced by looking at the peaks in the differential conductances traces $\mathrm{d}I/\mathrm{d}V(V)$, shown in Fig. 5(b). At the same time the Γ_α's determine the saturation current, as shown in Fig. 5(a). Our calculated I-V curves present a reduction of the conductance gap as the molecule is tilted towards the electrodes, i.e. as θ gets larger. This is determined by the drift of the HOMO towards $E_{\rm F}$ as the molecule approaches the electrodes, which in turn is determined by the image charge effect. These results are in qualitative agreement with experiments. The agreement becomes quantitative for angles in the range $\theta = 45^0 - 55^0$, indicating that configurations where the

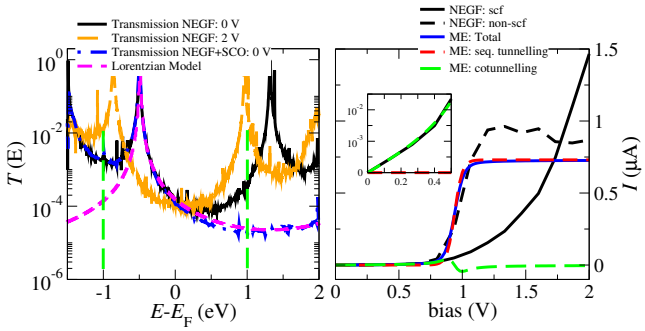

Figure 4: Transport properties of the thiol-terminated junction at the equilibrium position ($\theta = 0$). The transmission coefficient as a function of energy is shown in the left panel. In particular we present the LDA results at zero and finite bias, the LDA results after application of the scissor operator, and a fit to a Lorentzian model. The corresponding I-V curves are presented in the right panel. In addition the right panel shows the I-V curve calculated with the ME and the individual contributions arising from sequential tunnelling and cotunnelling.

molecule is tilted are explored in actual experiments. Note that in general the current is determined mainly by sequential tunnelling contributions, with those associated to cotunnelling being responsible for minor features in the current-voltage profile (see Fig. S1 in the supplementary information).

When one compares our calculated I-V curves with the experimental ones of Perrin *et al.*[1] a feature becomes notable, namely that the experimental current, I, does not saturate after its onset, but rather approximately grows linearly with the voltage. It has been shown in the past that such an effect in molecular junctions can be attributed to vibronic excitations.[53,54] In order to capture such feature of the I-V profile we include in our ME description the interaction between conduction electrons and molecular vibrations. The model is simplified by taking a single Holstein vibron of frequency ω_p coupled to the conduction electrons by the adimensional interaction strength, λ. DFT vibron calculations for the molecule in the gas phase reveal a high density of modes in the region 10-17 meV, most of which related to the breathing of the porphyrin ring. As such we consider here an average single vibron energy of $\hbar\omega_p = 10$ meV. The model is completed by introducing a phenomenological vibron life-time, τ, (see computational methods). Fig. 5(c) and Fig. 5(d) show respectively the I-V curves and the $\mathrm{d}I/\mathrm{d}V$ profile for three different experimental curves (dashed lines) compared to our calculated sequential tunnelling results (solid lines), when vibrons are considered. The experimental data are extracted from Ref. [1].

In our simulations the electron-vibron remains an adjustable parameter, and our results show that an intermediate value, $\lambda = 2$, returns very good qualitative agreement with the experiment data (dashed line). For weak

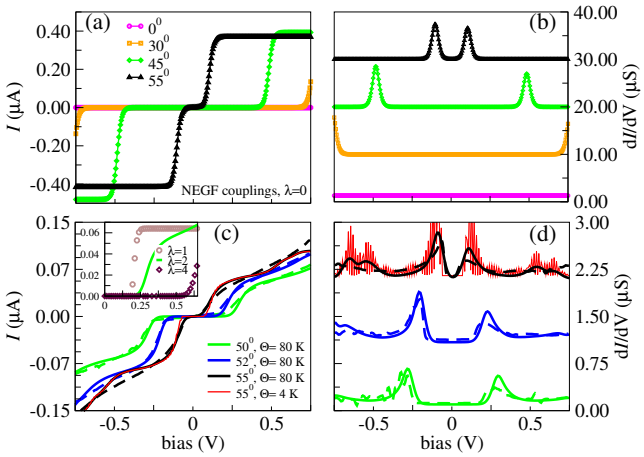

Figure 5: Transport properties of several thiol-terminated junctions for different binding angle, θ, as obtained from the ME: (a) sequential tunnelling current as a function of bias at a temperature $\Theta = 80$ K; (b) $\mathrm{d}I/\mathrm{d}V$. The values used for the Γ_α's are given in Table I, while the energy levels positions are from Fig. 3. In panel (c) the calculated sequential tunnelling I-V's (solid lines) are compared to the experimental data (dashed lines) and in panel (d) we show the corresponding $\mathrm{d}I/\mathrm{d}V$'s. The parameters used in (c) and (d) are: $\Theta = 80$ K; $\lambda = 2$; $\Gamma_{\mathrm{L(R)}} = 0.35(0.53)$ meV for $\theta = 50^0$; $\Gamma_{\mathrm{L(R)}} = 0.35(0.9)$ meV for $\theta = 52^0$ and $\Gamma_{\mathrm{L(R)}} = 0.35(0.8)$ meV for $\theta = 55^0$. For $\theta = 55^0$ the results are also shown at a low temperature of $\Theta = 4$ K (red-solid line). The inset in (c) shows the sequential tunnelling contribution for $\theta = 50^0$ for different values of λ.

electron-vibron coupling, $\lambda = 1$, vibrational excitations do not perturb the I-V curve enough and the current still saturate after the onset [see inset in Fig. 5(c)]. In contrast, strong electron-vibron coupling, $\lambda = 4$, leads to the so-called Franck-Condon blockade limit,[52,53,55] which has not been observed in the experiments of Perrin et al.[1] Further analysis is provided by performing calculation for different temperature, Θ. In particular we observe that for $\lambda = 2$ and $\Theta = 4$ K (the experimental temperature of the whole apparatus, which can be significantly different from the local temperature in the molecular junction) the peaks in the $\mathrm{d}I/\mathrm{d}V$ traces [red-solid curve in Fig. 5(d)] are not as sharp as those experimentally measured. This seems to suggest that local heating in the electrodes occurs in real experiments.

Our calculated Γ's given in Table I (i.e. $\Gamma_\alpha = 3.5 - 8$ meV) and used to calculate the current for the thiol-terminated junctions shown in Fig. 5(a) are one order of magnitude larger than the ones needed for a quantitative agreement with the experimental curves (i.e. $\Gamma_\alpha = 0.35 - 0.9$ meV), as shown in Fig. 5(c). Note that in Fig. 5(a) vibrations are not considered ($\lambda = 0$). The electronic couplings used to reproduce the experimental results are asymmetric, although of the same order of magnitude. This explains why the experimental curves are slightly asymmetric, which is expected in realistic experimental conditions. In order to understand the origin of this disagreement we have performed two other sets of calculations, where the molecule is attached to two tip-shaped electrodes, as shown in Fig. 1(c-d). In the first configuration the molecule is attached to the apexes of the two tips, whereas in the second one it lays flat on top of the two. Such second geometry simulates a possible compressed configuration where the molecule slides on top of the electrodes.

For the geometry shown in Fig. 1(c) we observe a reduction in the electronic couplings by a factor four when compared to the flat electrodes, whereas for the geometry shown in Fig. 1(d) the electronic couplings are reduced by about a factor two. We have also performed transport calculations for the flat and tip electrodes, where we increase symmetrically the distance between the linking group and the gold atom with respect to the equilibrium distance. We have then extracted the electronic couplings for the HOMO level as a function of the S-Au distance, see Fig. S3 in the SI. In both cases we observe a reduction of the electronic coupling of the HOMO by 20% when we increase the S-Au bond length by 0.5 Å. This reduces the saturation current by the same amount, since the sequential tunnelling contribution to the current is proportional to the electronic couplings. These findings indicate that changes in the contact geometry calculated with ground state DFT do not lead to the substantial reduction of the electronic couplings needed for a quantitative comparison with experiment.

We note that also the relative angle between the side phenyl rings attached to the sulfur atoms and the main porphyrin ring can substantially affect the electronic coupling between the HOMO and the electrodes. We have then performed transport calculations, where these rings are rotated to be parallel to the main porphyrin one (not shown). The positions of the energy levels with respect to E_{F} change, as well as the electronic coupling. In fact, the Γ_α is now 24 meV for the HOMO, which is about four times larger than the one presented in Table I. This is related to the enhanced alignment of the π orbitals of the porphyrin with the π orbitals of the side phenyl rings attached to the S atoms, as shown in the SI, Fig. S5(c-d). Such a higher-energy configuration is unlikely to appear in experiment, since it does not correspond to the relaxed ground state geometry.

Recently, many-body calculations based on the GW approximation have shown that by considering dynamical effects to the image charge formation, the electronic couplings can be reduced by 15% compared to the static case.[56] These minor corrections are therefore not expected to significantly modify our *ab initio* results. At the same time it has been shown that temperature effects[13,14,57] can suppress the linear conductance. Berritta *et al.*[57], by means of molecular dynamics calculations at 300 K for the same tip-shaped electrodes and the same anchoring group, have shown that the linear conductance can be reduced by two orders of magnitude when compared to ground-state LDA-DFT calculations. This in-

dicates that the current-induced local heating leads not only to the slope in the *I-V* curves above the onset of current, but that it might also lead to an effective reduction of the electronic couplings. The Hostein model used in the present work captures the change in the onsite energy due to changes in the structure of the molecule when an electron is added to the it. We note that vibrations that significantly affect the molecule-electrode bond geometry can also play an important role, in particular in evaluating the effective molecule-electrodes electronic coupling parameters.

In conclusion we have presented a combination of DFT-NEGF formalism and ME approach to study the transport properties of molecular junctions. The benefit of our approach is that it can tackle the weak coupling limit while remaining full *ab initio*, since all the parameters needed by the ME are extracted from first-principles calculations. We have applied this combined approach to a case where both energy levels renormalization and vibronic excitations play a crucial role in determining the *I-V* curve profile.

I. COMPUTATIONAL METHODS

All the *ab initio* calculations presented here are based on DFT as implemented in the SIESTA package.[58] The exchange and correlation energy is treated at the level of LDA. We use norm-conserving pseudopotentials according to the Troullier-Martins procedure[59] and the basis set is double-ζ polarized for carbon, sulphur and hydrogen and single-ζ for gold. This is a standard basis for transport calculations.[13,14] The real-space equivalent mesh cutoff is 300 Ry and four k-points are used for the Brillouin zone sampling in the plane perpendicular to the transport direction. For the *ab-initio* quantum transport calculations, we use the NEGF scheme as implemented in the SMEAGOL code (see SI for more details).[60,61]

Model Hamiltonian and master equations. We define the Hamiltonian of the entire system (molecule plus electrodes) as

$$\hat{H} = \hat{H}_{\rm mol} + \hat{H}_{\rm L} + \hat{H}_{\rm R} + \hat{H}_{\rm T}\,, \qquad (2)$$

where the part describing the molecule is given by the Anderson-Holstein model

$$\hat{H}_{\rm mol} = \sum_i^M \epsilon_i \hat{n}_i + \sum_i^M \frac{\mathcal{U}_i}{2}\hat{n}_i\left(\hat{n}_i - 1\right) + \hbar\omega_p\left(\hat{b}^\dagger\hat{b} + 1/2\right) + \sum_i^M \lambda\hbar\omega_p\left(\hat{b}^\dagger + \hat{b}\right)\hat{n}_i, \qquad (3)$$

for i-th single-particle states of energy ϵ_i and charging energy $\mathcal{U}_i$. Here $\hat{n}_i = \sum_\sigma \hat{c}^\dagger_{i\sigma}\hat{c}_{i\sigma}$ is the number operator with $\hat{c}^\dagger_{i\sigma}(\hat{c}_{i\sigma})$ creating (annihilating) an electron in the molecular state i with spin σ. The Hamiltonian describing the α-th electrode is $\hat{H}_\alpha = \sum_{\alpha\mathbf{k}\sigma}\epsilon_{\alpha\mathbf{k}\sigma}\hat{d}^\dagger_{\alpha\mathbf{k}\sigma}\hat{d}_{\alpha\mathbf{k}\sigma}$, where $\alpha = {\rm L,R}$. In this case $\hat{d}^\dagger_{\alpha\mathbf{k}\sigma}$ ($\hat{d}_{\alpha\mathbf{k}\sigma}$) creates (annihilates) an electron with momentum $\mathbf{k}$ and spin σ on the α-th electrode. The third and fourth terms in Eq. (3) describe respectively a single vibronic degree of freedom of energy $\hbar\omega_p$ ($\hbar$ is the Planck's constant), and the electron-vibron coupling with non-dimensional coupling constant λ. Here $\hat{b}^\dagger(\hat{b})$ is the creation (annihilation) bosonic operator for the vibrational mode. Finally the interaction between the electrodes and the molecule is given by the tunnelling Hamiltonian $\hat{H}_{\rm T} = \sum_{\alpha i\mathbf{k}}\left[\gamma_\alpha\hat{c}^\dagger_i\hat{d}_{\alpha\mathbf{k}} + \gamma^*_\alpha\hat{c}_i\hat{d}^\dagger_{\alpha\mathbf{k}}\right]$, with tunnelling amplitude γ_α. This is treated perturbatively in our ME approach. The electron-vibron coupling term can be eliminated by canonical transformation,[52,62,63] leading to a renormalization of $\epsilon_i \to \tilde{\epsilon}_i = \epsilon_i - \lambda^2\hbar\omega_p$ and $\mathcal{U}_i \to \tilde{\mathcal{U}}_i = \mathcal{U}_i - 2\lambda^2\hbar\omega_p$. It has also been shown that electron-phonon coupling may lead to band gap renormalization in solids.[64] For simplicity, we do not allow a second electron in the molecule, i.e. $\tilde{\mathcal{U}}_i \to \infty$. Such transformation introduces a translation operator into the tunnelling matrix elements $\gamma_\alpha \to \gamma_\alpha{\rm exp}[-\lambda(\hat{b}^\dagger - \hat{b})]$.[52] Within the $\mathscr{T}$-matrix[44,65–67] approach one evaluates the diagonal terms of the reduced density matrix, which are given by[44,68]

$$\dot{\rho}^q_m(t) = \sum_{\alpha\alpha';m}\left(\Gamma^{nm;q'q}_{\alpha\alpha'}\rho^{q'}_n - \Gamma^{mn;qq'}_{\alpha\alpha'}\rho^q_m\right) + \frac{1}{\tau}\left(\rho^q_m - \rho^q_{\rm eq}\sum_{q'}\rho^{q'}_n\right), \qquad (4)$$

where ρ^q_m is the occupation of the state $|m,q\rangle$ and m and q are respectively the charge and the vibronic quantum numbers of the molecule. The transition rates, $\Gamma^{mn,qq'}_{\alpha\alpha'}$ are given by the generalized Fermi's golden rule. This is expanded up to fourth order in $\hat{H}_{\rm T}$ in order to account for sequential and cotunnelling processes (see SI for more details).[68] The second term of Eq. (4) is added phenomenologically and describes relaxation of vibrons towards their thermal equilibrium distribution $\rho^q_{\rm eq} = e^{-q\hbar\omega_p/k_{\rm B}\Theta}(1 - e^{-\hbar\omega_p/k_{\rm B}\Theta})$. The time scale for such relaxation is determined by the parameter τ. For $\tau \to \infty$ the system never thermalises, whereas for $\tau \to 0$ it relaxes instantaneously to the vibronic ground state. In the present work we use $\tau = 1$ ps, which is of the same order of magnitude as values measured in closely related systems[69,70], while the cutoff vibron population is set to $q_{\rm max} = 120$ (see Fig. S4 in the SI for details).

II. SUPPORTING INFORMATION

Details of the master equation approach, the scissor operator method and the procedure used to extract the electronic couplings are available as Supplementary Material. This is available free of charge at http://pubs.acs.org.

Acknowledgments

The authors are thankful to the King Abdullah University of Science and Technology (Kingdom of Saudi Arabia) for the financial support through the ACRAB project, to the Trinity College High-Performance Computer Center (TCHPC) and the Ireland's High-Performance computing centre (ICHEC) for computational resources. Additional support was provided by the European Research Council (Quest and HINTS projects).

[1] M. L. Perrin, C. J. O. Verzijl, C. A. Martin, A. J. Shaikh, R. Eelkema, J. H. van Esch, J. M. van Ruitenbeek, J. M. Thijssen, H. S. J. van der Zant, and D. Dulić, "Large tunable image-charge effects in single-molecule junctions", *Nature Nanotechnology* **8**, pp. 282–287 (2013).

[2] M. A. Reed, C. Zhou, C. J. Muller, T. P. Burgin, and J. M. Tour, "Conductance of a molecular junction", *Science* **278**, pp. 252–254 (1997).

[3] E. Lörtscher, H. Weber, and H. Riel, "Statistical approach to investigating transport through single molecules", *Phys. Rev. Lett.* **98**, pp. 176807–176811 (2007).

[4] M. T. Gonzalez, S. Wu, R. Huber, S. J van der Molen, C. Schönenberger, and M. Calame, "Electrical conductance of molecular junctions by a robust statistical analysis.", *Nano Lett.* **6**, pp. 2238–2242 (2006).

[5] Y. Kim, T. Pietsch, A. Erbe, W. Belzig, and E. Scheer, "Benzenedithiol: a broad-range single-channel molecular conductor.", *Nano Lett.* **11**, pp. 3734–3738 (2011).

[6] M. Taniguchi, M. Tsutsui, K. Yokota, and T. Kawai, "Mechanically-controllable single molecule switch based on configuration specific electrical conductivity of metal-moleculemetal junctions", *Chem. Sci.* **1**, pp. 247–253 (2010).

[7] Jing-Hua Tian, B. Liu, X. Li, Zhi-Lin Yang, B. Ren, Sun-Tao Wu, N. Tao, and Zhong-Qun Tian, "Study of molecular junctions with a combined surface-enhanced Raman and mechanically controllable break junction method.", *J. Am. Chem. Soc.* **128**, pp. 14748–14749 (2006).

[8] Jing-Hua Tian, Y. Yang, Xiao-Shun Zhou, B. Schöllhorn, E. Maisonhaute, Zhao-Bin Chen, Fang-Zu Yang, Y. Chen, C. Amatore, Bing-Wei Mao, and Zhong-Qun Tian, "Electrochemically assisted fabrication of metal atomic wires and molecular junctions by MCBJ and STM-BJ methods.", *Chemphyschem* **11**, pp. 2745–2755 (2010).

[9] M. Tsutsui, M. Taniguchi, K. Shoji, K. Yokota, and T. Kawai, "Identifying molecular signatures in metal-molecule-metal junctions.", *Nanoscale* **1**, pp. 164–170 (2009).

[10] M. Tsutsui, Y. Teramae, S. Kurokawa, and A. Sakai, "High-conductance states of single benzenedithiol molecules", *Appl. Phys. Lett.* **89**, pp. 163111–163113 (2006).

[11] M. Tsutsui, M. Taniguchi, and T. Kawai, "Atomistic mechanics and formation mechanism of metal - molecule - metal junctions", *Nano Lett.* **9**, pp. 2433–2439 (2009).

[12] A. M. Souza, I. Rungger, R. B. Pontes, A. R. Rocha, A. J. R. da Silva, U. Schwingenschlöegl, and S. Sanvito, "Stretching of BDT-gold molecular junctions: thiol or thiolate termination?", *Nanoscale* **6**, pp. 14495–14507 (2014).

[13] W. R. French, C. R. Iacovella, I. Rungger, A. M. Souza, S. Sanvito, and P. T. Cummings, "Structural origins of conductance fluctuations in gold - thiolate molecular transport junctions", *J. Phys. Chem. Lett.* **4**, pp. 887–891 (2013).

[14] W. R. French, C. R. Iacovella, I. Rungger, A. M. Souza, S. Sanvito, and P. T. Cummings, "Atomistic simulations of highly conductive molecular transport junctions under realistic conditions.", *Nanoscale* **5**, pp. 3654–3659 (2013).

[15] B. Muralidharan, A. W. Ghosh, S. K. Pati, and S. Datta, "Theory of high bias coulomb blockade in ultrashort molecules", *IEEE Trans. Nanotechnol.* **6**, pp. 536–544 (2007).

[16] R. Hesper, L. H. Tjeng, and G. A. Sawatzky, "Strongly reduced band gap in a correlated insulator in close proximity to a metal", *Eur. Lett.* **40**, pp. 177–182 (1997).

[17] J. Repp, G. Meyer, S. Stojković, A. Gourdon, and C. Joachim, "Molecules on insulating films: scanning-tunneling microscopy imaging of individual molecular orbitals", *Phys. Rev. Lett.* **94**, pp. 026803–026807 (2005).

[18] X. Lu, M. Grobis, K. H. Khoo, S. G. Louie, and M. F. Crommie, "Charge transfer and screening in individual C60 molecules on metal substrates: A scanning tunneling spectroscopy and theoretical study", *Phys. Rev. B* **70**, pp. 115418–115426 (2004).

[19] M. T. Greiner, M. G. Helander, Wing-Man Tang, Zhi-Bin Wang, J. Qiu, and Zheng-Hong Lu, "Universal energy-level alignment of molecules on metal oxides", *Nat. Mater.* **11**, pp. 76–81 (2011).

[20] A. M. Souza, I. Rungger, C. D. Pemmaraju, U. Schwingenschloegl, and S. Sanvito, "Constrained-DFT method for accurate energy level alignment of metal / molecule interfaces", *Phys. Rev. B* **88**, pp. 165112–165121 (2013).

[21] Y. Meir and S. W. Ned, "Landauer Formula for the Current through an Interacting electron Region", *Phys. Rev. Lett.* **68**, pp. 2512–2515 (1992).

[22] M. Di Ventra, *Electrical Transport in Nanoscale Systems*, Cambridge University Press New York (2008).

[23] M. Brandbyge, José-Luis Mozos, P. Ordejón, J. Taylor, and K. Stokbro, "Density-functional method for nonequilibrium electron transport", *Phys. Rev. B* **65**, pp. 165401–165418 (2002).

[24] W. Kohn and L. J. Sham, "Self-consistent equations including exchange and correlation effects", *Phys. Rev.* **140**, pp. A1133–A1138 (1965).

[25] P. Hohemberg and W. Kohn, "Inhomogeneus electron gas", *Phys. Rev.* **136**, pp. B864–B870 (1964).

[26] D. M. Ceperley and B. J. Alder, "Ground state of the electron gas by a stochastic method", *Phys. Rev. Lett.* **45**, pp. 566–569 (1980).

[27] J. P. Perdew, K. Burke, and M. Ernzerhof, "Generalized gradient approximation made simple", *Phys. Rev. Lett.* **77**, pp. 3865–3868 (1996).

[28] P. J. Stephens, F. J. Devlin, C. F. Chabalowski, and M. J. Frisch, "Ab initio calculation of vibrational absorption and circular dichroism spectra using density functional force fields", *J. Phys. Chem.* **98**, pp. 11623–11627 (1994).

[29] J. P. Perdew and A. Zunger, "Self-interaction correction to density-functional approximations for many-electron systems", *Phys. Rev. B* **23**, pp. 5048–5079 (1981).
[30] C. D. Pemmaraju, T. Archer, D. Sánchez-Portal, and S. Sanvito, "Atomic-orbital-based approximate self-interaction correction scheme for molecules and solids", *Phys. Rev. B* **75**, pp. 045101–045117 (2007).
[31] P. Darancet, J. R. Widawsky, H. J. Choi, L. Venkataraman, and J. B. Neaton, "Quantitative current?voltage characteristics in molecular junctions from first principles", *Nano Lett.* **12**, pp. 6250–6254 (2012).
[32] J. M. Garcia-Lastra, C. Rostgaard, A. Rubio, and K. S. Thygesen, "Polarization-induced renormalization of molecular levels at metallic and semiconducting surfaces", *Phys. Rev. B* **80**, pp. 245427–245434 (2009).
[33] M. Strange, C. Rostgaard, H. Häkkinen, and K. S. Thygesen, "Self-consistent GW calculations of electronic transport in thiol- and amine-linked molecular junctions", *Phys. Rev. B* **83**, pp. 115108–115120 (2011).
[34] J. B. Neaton, Mark Hybertsen, and S. G. Louie, "Renormalization of Molecular Electronic Levels at Metal-Molecule Interfaces", *Phys. Rev. Lett.* **97**, pp. 216405–216410 (2006).
[35] J. P. Perdew, R. G. Parr, M. Levy, and J. L. Balduz, "Density functional theory for fractional particle number: derivative discontinuities of the energy", *Phys. Rev. Lett.* **49**, pp. 1691–1694 (1982).
[36] J. P. Perdew and M. Levy, "Physical content of the exact Kohn-Sham orbital energies: band gaps and derivative discontinuities", *Phys. Rev. Lett.* **51**, pp. 1884–1887 (1983).
[37] L. J. Sham and M. Schluter, "Density-functional theory of the energy gap", *Phys. Rev. Lett.* **51**, pp. 1888–1891 (1983).
[38] B. Song, "DFT-based calculation of Coulomb blockade in molecular junction", *arXiv:0710.0475v1* (2007).
[39] Z. Yu, J. Chen, L. Zhang, and J. Wang, "First-principles investigation of quantum transport through an endohedral N@C_{60} in the Coulomb blockade regime", *Journal of Phys.: Cond. Matter* **25**, pp. 495302–495309 (2013).
[40] C. Toher, A. Filippetti, S. Sanvito, and K. Burke, "Self-interaction errors in density-functional calculations of electronic transport", *Phys. Rev. Lett.* **95**, pp. 146402 (2005).
[41] T. Hansen, V. Mujica, and M. A. Ratner, "Cotunneling model for current-induced events in molecular wires", *Nano Lett.* **8**, pp. 3525–3531 (2008).
[42] J. N. Pedersen and A. Wacker, "Modeling of cotunneling in quantum dot systems", *Phys. E Low-dimensional Syst. Nanostructures* **42**, pp. 595–599 (2010).
[43] M. Turek and K. Matveev, "Cotunneling thermopower of single electron transistors", *Phys. Rev. B* **65**, pp. 115332–1153341 (2002).
[44] F. Elste and C. Timm, "Cotunneling and nonequilibrium magnetization in magnetic molecular monolayers", *Phys. Rev. B* **75**, pp. 195341–195349 (2007).
[45] C. D. Pemmaraju, I. Rungger, and S. Sanvito, "*Ab initio* calculation of the bias-dependent transport properties of mn_{12} molecules", *Phys. Rev. B* **80**, pp. 104422–104431 (2009).
[46] A. J. Cohen, P. Mori-Sánchez, and W. Yang, "Insights into current limitations of density functional theory.", *Science* **321**, pp. 792–796 (2008).
[47] R. O. Jones and O. Gunnarsson, "The density functional formalism, its applications and prospects", *Rev. Mod. Phys.* **61**, pp. 689–746 (1989).
[48] S. Y. Quek, L. Venkataraman, H. J. Choi, S. G. Louie, M. S. Hybertsen, and J. B. Neaton, "Amine-gold linked single-molecule circuits: experiment and theory.", *Nano Lett.* **7**, pp. 3477–3482 (2007).
[49] S. Y. Quek, H. J. Choi, S. G. Louie, and J. B. Neaton, "Thermopower of Amine - Gold-Linked Principles", *ACS nano* **1**, pp. 551–557 (2011).
[50] V. M. García-Suárez and C. J. Lambert, "First-principles scheme for spectral adjustment in nanoscale transport", *New J. Phys.* **13**, pp. 53026–53042 (2011).
[51] S. Datta, *Quantum Transport: Atom to Transistor*, Cambridge University Press, Cambridge (2005).
[52] J. Koch, F. von Oppen, and A. V. Andreev, "Theory of the Franck-Condon blockade regime", *Phys. Rev. B* **74**, pp. 205438–205457 (2006).
[53] J. Koch and F. von Oppen, "Franck-Condon blockade and giant fano factors in transport through single molecules", *Phys. Rev. Lett.* **94**, pp. 206804–206808 (2005).
[54] H. Park, J. Park, A. K. L. Lim, E. H. Anderson, A. P. Alivisatos, and P. L. McEuen, "Nanomechanical oscillations in a single-C 60 transistor", *Nature* **407**, pp. 57–60 (2000).
[55] E. Burzur, Y. Yamamoto, M. Warnock, X. Zhong, K. Park, A. Cornia, and H. S. J. van der Zant, "Franck-Condon blockade in a single-molecule transistor", *Nano Lett.* **14**, pp. 3191–3196 (2014).
[56] C. Jin and K. S. Thygesen, "Dynamical image-charge effect in molecular tunnel junctions: beyond energy level alignment", *Phys. Rev. B* **89**, pp. 041102R–041107R (2014).
[57] M. Berritta, D. Z. Manrique, and C. J. Lambert, "Interplay between quantum interference and conformational fluctuations in single-molecule break junctions", *Nanoscale* **7**, pp. 1096–1101 (2014).
[58] M. S. Soler, E. Artacho, J. D. Gale, A. García, J. Junquera, Pablo Ordejón, and Sánchez-Portal Daniel, "The SIESTA method for ab initio order- N materials", *J. Phys. Condens. Matter* **14**, pp. 2745–2779 (2002).
[59] N. Troullier and J. L. Martins, "Efficient pseudopotentials for plane-wave calculations", *Phys. Rev. B* **43**, pp. 1–14 (1993).
[60] A. R. Rocha, V. M. García-Suárez, S. Bailey, C. Lambert, J. Ferrer, and S. Sanvito, "Spin and molecular electronics in atomically generated orbital landscapes", *Phys. Rev. B* **73**, pp. 85414–85435 (2006).
[61] I. Rungger and S. Sanvito, "Algorithm for the construction of self-energies for electronic transport calculations based on singularity elimination and singular value decomposition", *Phys. Rev. B* **78**, pp. 035407–035420 (2008).
[62] D. C. Langreth, "Singularities in the X-Ray spectra of metals", *Phys. Rev. B* **108**, pp. 471–477 (1970).
[63] A. Mitra, I. Aleiner, and A. J. Millis, "Phonon effects in molecular transistors:?quantal and classical treatment", *Phys. Rev. B* **69**, pp. 245302–245324 (2004).
[64] F. Giustino, S. G. Louie, and M. L. Cohen, "Electron-phonon renormalization of the direct band gap of diamond", *Phys. Rev. Lett.* **105**, pp. 265501–265506 (2010).
[65] C. Timm, "Tunneling through molecules and quantum dots: master-equation approaches", *Phys. Rev. B* **77**, pp. 195416–195429 (2008).
[66] G. Begemann, S. Koller, M. Grifoni, and J. Paaske, "Inelastic cotunneling in quantum dots and molecules with weakly broken degeneracies", *Phys. Rev. B* **82**, pp. 045316–045327 (2010).
[67] S. Koller, M. Grifoni, M. Leijnse, and M. R. Wegewijs,

"Density-operator approaches to transport through interacting quantum dots: simplifications in fourth order perturbation theory", *Phys. Rev. B* **82**, pp. 235307–235334 (2012).

[68] J. Koch, F. von Oppen, Y. Oreg, and E. Sela, "Thermopower of single-molecule devices", *Phys. Rev. B* **70**, pp. 195107–195129 (2004).

[69] J. Helbing and et. al., "Time-resolved visible and infrared study of the cyano complexes of myoglobin and hemoglobin I from *lucina pectinata*", *Biophysical Journal* **87**, pp. 1881–1891 (2004).

[70] T. Lian and et. al., "Energy flow from solute to solvent probed by fentosencond IR spectroscopy: malachite green and heme protein solutions", *J. Phys. Chem.* **98**, pp. 11648–11656 (1994).